

New Insights Into Achievable Spectral Efficiency With Adaptive Free Space Optical Transmissions

Himani Verma, Kamal Singh, and Ranjan K. Mallik, *Fellow, IEEE*

Abstract—Terrestrial free-space optical (FSO) communication systems, while designed to operate on large unlicensed optical bandwidths, are power-constrained due to strict eye safety regulations. The channel fluctuation inherent in terrestrial FSO links also limits the received optical power. Consequently, the available signal-to-noise ratio (SNR) per Hz could become limited; this holds for future long-haul terrestrial systems based on coherent optical communications. An efficient and adaptive transmission mechanism is thus crucial at the optical source. However, a critical assessment of the impact of adaptive transmission in terrestrial FSO systems has received less attention in the literature. This work studies terrestrial FSO communication systems employing adaptive beam transmission while detection receivers operate under shot noise-limited conditions. Specifically, we propose a novel exact closed-form expression for the average spectral efficiency of these FSO systems with transmit beam power adaptation over the gamma-gamma turbulence channel with pointing error. More importantly, we provide a detailed assessment of the impact of turbulence and pointing error impairments on the performance of the aforementioned FSO systems, revealing several novel and counterintuitive insights. In particular, the extensive numerical results help elucidate the intricacies of analyzing these terrestrial FSO systems and clarify a few misconceptions alluded to in recent related literature.

Index Terms—Average spectral efficiency, free-space optical (FSO) communications, optical beam power adaptation, gamma-gamma turbulence, pointer error, shot noise.

I. INTRODUCTION

Laser-based free-space optical (FSO) communication has gained significant attention as a viable alternative to conventional radio-frequency (RF) and fiber-optic technologies for delivering efficient backhaul connectivity in outdoor wireless networks. This growing interest is driven by several inherent advantages of FSO systems, including the availability of vast unlicensed bandwidth, ease of deployment, inherent physical-layer security, and low-cost transceiver implementation [1]. Consequently, the scope of FSO-based wireless technologies has broadened considerably, finding applications in a wide range of scenarios such as ad hoc wireless networks for tactical and emergency response situations [1], terrestrial last-mile broadband access [2], deep-space communications [3], inter-satellite links [4], and various civil and military operations [5]. In particular, the demand for ultra-high data rates in next-generation wireless networks, including 5G and 6G systems, has spurred renewed interest in coherent FSO technologies, with recent terrestrial demonstrations achieving net data rates exceeding 400 Gbps [6], [7], and 800 Gbps per channel [8].

Himani Verma and Kamal Singh are with the Department of Electrical Engineering, Shiv Nadar Institution of Eminence, Delhi NCR, 201314, India (e-mail: hv790@snu.edu.in; kamal.singh@snu.edu.in).

Ranjan K. Mallik is with the Department of Electrical Engineering, Indian Institute of Technology, Delhi, Haus Khas, New Delhi 110016, India (email: rkmallik@ee.iitd.ernet.in).

Detection schemes in most practical FSO communication systems fall into two main categories:

(i) Intensity modulation with direct detection (IM-DD): In this modulation-detection scheme, information is encoded in the intensity of the transmitted optical beam, effectively utilizing only *one degree of freedom*. At the receiver, the optical signal is detected directly via its impingement on a photodetector. IM-DD is favored in commercial systems due to its simplicity and low-cost implementation but suffers from limited receiver sensitivity, restricting its use to short-range terrestrial links [9], [10].

(ii) Coherent heterodyne detection (HD): Coherent systems exploit both the amplitude and phase of the optical carrier to convey information, enabling *two degrees of freedom*. In heterodyne detection, a locally generated optical signal—typically offset in frequency from the received signal—is mixed with the incoming beam prior to photodetection. This approach significantly improves receiver sensitivity, which can be leveraged to extend link distances. Additionally, coherent receivers enable high selectivity via narrowband RF filtering, in contrast to the broader optical filtering in IM-DD systems [10].

Despite their numerous advantages, terrestrial FSO communication systems face two primary practical challenges. First, FSO links are highly sensitive to atmospheric effects: rapid channel fluctuations induced by turbulence, and slower attenuation due to scattering and absorption [11]. Second, since FSO communication relies on *line-of-sight* (LOS) alignment with highly directional laser beams and photodetectors, it is vulnerable to pointing errors. These errors can arise from various physical disturbances such as wind-induced vibrations, transmitter-receiver misalignment due to motion, thermal expansion, or structural sway of buildings. In practice, the severity of such errors depends strongly on the acquisition, tracking, and pointing (ATP) subsystem, which mitigates beam misalignment but cannot fully eliminate residual jitter [11]. Either or both of these impairments can significantly degrade the performance and reliability of FSO systems [12].

Several statistical models for the small-scale intensity fluctuations are available in the FSO communication literature with a strong basis in realistic terrestrial propagation conditions. We mention a select few important and relevant models as follows: scintillation in weak turbulence is well modeled using log-normal distribution [13], [14], while the scintillation statistic in the weak-to-strong turbulence regimes is best described by gamma-gamma (GG) distribution [14]. Pointing errors due to jitter are addressed in [15] and extended to nonzero bore-sight in [16]. More recently, generalized turbulence models such as Málaga (\mathcal{M}) [17], double-generalized gamma [18], and Fisher-Snedecor \mathcal{F} [19] have been introduced, offering enhanced flexibility across diverse channel conditions.

Transmit optical power in terrestrial FSO communications is limited by stringent eye and skin safety regulations [20]. In contrast, FSO links benefit from virtually unlimited optical bandwidths (tens to hundreds of gigahertz per wavelength) to support ultra-high-speed communications [12], making the available power per hertz a potential limiting factor. While such low-SNR operating points are rarely encountered today, recent demonstrations of extreme-wideband wavelength-division multiplexing (WDM) coherent FSO systems indicate that distributing a fixed transmit power over many carriers may plausibly lead to lower per-channel SNR [7], [21]. In addition, variability in atmospheric attenuation under haze, fog, or pollution can accentuate this effect. Thus, operation in the low-SNR regime may emerge as a relevant consideration for future ultra-wideband WDM terrestrial FSO systems. In addition, irradiance fluctuations (mentioned earlier) present in terrestrial FSO channels degrade the power collected at the receiver [11], but this degradation can be alleviated through power control. For instance, a simple scheme in which the transmitter activates only when the instantaneous channel quality exceeds a predefined threshold can be effective under low-power budgets. Importantly, typical terrestrial FSO channels exhibit extremely high coherence bandwidths (hundreds of gigahertz or more) [22], [23] and relatively long coherence times on the order of milliseconds [24]. These conditions yield a quasi-static, frequency-flat block-fading channel, which is increasingly exploited by recent field trials [6], [7], [8], [21] for adaptive transmission in terrestrial coherent FSO links. This context motivates the subsequent analysis of spectral efficiency in low-SNR regimes, where turbulence-induced fluctuations and limited per-Hz transmit power, especially in ultra-wideband WDM coherent FSO systems, can meaningfully affect achievable throughput.

In contrast to the recent practical advances mentioned above, adaptive terrestrial FSO communication systems have attracted comparatively limited rigorous theoretical analysis in the literature, as summarized next. Prior works on IM-DD and coherent HD based terrestrial FSO communication systems have examined achievable spectral efficiency (SE) under log-normal and gamma-gamma (GG) turbulence models (e.g., [25], [26], [27], [28], [29], [30], and references therein). More recent studies have extended this analysis to generalized turbulence channels, such as those modeled by the double-generalized gamma and Málaga (\mathcal{M}) distributions [31], [32], [33], [34]. Despite these contributions, the critical aspect of beam power adaptation at the optical transmitter has been largely overlooked—except in a few cases, such as [25], [26], and [27]. This omission is likely due to the analytical complexity involved in solving the associated optimization problems. In [26], an infinite series solution for the SE of an HD-based adaptive FSO system operating over GG turbulence is presented; however, this approach introduces concerns related to truncation error and interpretability. Exact and asymptotic SE expressions for IM-DD-based adaptive systems under thermal noise-limited GG channels are derived in [25]–[27]. Notably, these works do not address the inherent non-convexity of the SE maximization problem in this regime (see Remark 2), a critical oversight that affects the validity of the reported results.

Furthermore, the authors in [32] present a unified SE expression for IM-DD and HD based FSO communication under the \mathcal{M} distribution, which includes the GG distribution as a special case; however, this analysis assumes a fixed transmit beam power, without adaptation. It is also important to note that several FSO related studies [25], [28], [29], [31], [32] lack clarity in the methodology used to simulate varying turbulence conditions. In terrestrial FSO systems, several channel parameters are interdependent—for example, changes in the FSO link length simultaneously affect turbulence severity level, path loss, and pointing error statistics. A rigorous understanding of these interrelations grounded in physical modeling is crucial for accurately evaluating FSO system performance. Neglecting such dependencies may lead to misleading interpretations and flawed insights.

To address these research gaps in terrestrial FSO research, we will utilize adaptive optical signal transmission on existing terrestrial FSO communication systems with an emphasis on spectral efficiency improvement, which basically relies on exploiting the temporal channel fluctuations due to turbulence and pointing error impairments. Specifically, this work aims to provide in-depth insights into the operation of terrestrial FSO communication systems, and provide a baseline SE performance for future adaptive FSO systems with strong practical constraints.

The principal contributions of this paper are summarized as follows.

- We present a novel, unified, and exact closed-form expression for the average spectral efficiency (ASE) of beam power adaptation-based FSO communication systems with IM-DD and HD receivers, accounting for gamma-gamma (GG) turbulence and pointing error impairments. Theorem 1, along with its specialization in Corollary 1 for the case without pointing errors, represents the central analytical contribution of this work.
- The accuracy of the derived closed-form ASE expressions is firmly established through extensive Monte Carlo simulations, demonstrating consistent agreement over wide and practically relevant ranges of signal-to-noise ratios (SNRs), turbulence strength, and pointing error conditions, as illustrated in Figures 1-2.
- To provide deeper insight into the influence of turbulence and pointing errors on adaptive FSO system performance, the exact ASE is further examined in the asymptotic regimes of both high and low SNR regimes. Theorem 2 characterizes these limiting behaviors in detail, thereby providing clear insights into the performance gains achievable as well as the penalties incurred under practical terrestrial FSO links.
- Among the several concrete findings, two particularly noteworthy and counterintuitive results are highlighted: i) at high SNRs, the ASE of the optical channel improves with turbulence when strong pointing error condition is considered (cf. Fig. 2); and ii) at low SNRs, the ASE of the terrestrial FSO channel improves with turbulence (cf. Fig. 5). These phenomena are rigorously characterized and analytically justified.

The remainder of this paper is organized as follows. The opti-

cal turbulence and pointing error models adopted for terrestrial FSO channel are presented in Subsection II-A. The relevant noise sources and the considered FSO receiver models are described in Subsections II-B and II-C, respectively. Theorems on the spectral efficiency of the turbulent optical channel are derived in Section III and their extensive numerical analysis is presented in Section IV. Finally, Section V summarizes the main results and provides concluding remarks along with directions for future work.

II. CHANNEL AND SYSTEM MODELS

A. Gamma–Gamma Turbulence with Pointing Error

The overall intensity fluctuation, or fading, I , of a transmitted laser beam due to atmospheric turbulence and pointing error is modeled as

$$I = I_l I_a I_p \quad (1)$$

where I_l represents the path loss component, determined by the exponential Beer-Lambert law for a given link length and weather conditions [35], I_a accounts for turbulence-induced fluctuations, and I_p corresponds to pointing-error-induced fluctuations. In this work, we assume $I_l = 1$. The statistical models for these independent fading components are described next.

Gamma–Gamma Turbulence: The statistics of the intensity fluctuation I_a , which spans the weak-to-strong turbulence regimes, are well modeled by the gamma-gamma distribution:

$$f_{I_a}(I_a) = \frac{2(ab)^{(a+b)/2}}{\Gamma(a)\Gamma(b)} I_a^{(a+b)/2-1} K_{a-b} \left(2\sqrt{abI_a} \right); I_a > 0 \quad (2)$$

where a and b are the shape parameters [14], $\Gamma(\cdot)$ is the Gamma function [36, Eq. (8.310.1)], and $K_\nu(\cdot)$ is the modified Bessel function of the second kind and order ν [36, Eq. (8.494.1)]. For plane wave optical radiation at the receiver, the GG parameters a and b are related to atmospheric conditions as

$$a = \left[\exp(0.49\sigma_R^2 / (1 + 1.11\sigma_R^{12/5})^{7/6}) - 1 \right]^{-1}, \quad (3)$$

$$b = \left[\exp(0.51\sigma_R^2 / (1 + 0.69\sigma_R^{12/5})^{5/6}) - 1 \right]^{-1}, \quad (4)$$

where $\sigma_R^2 = 1.23 C_n^2 k_w^{7/6} L^{11/6}$ is the Rytov variance determining the atmospheric turbulence strength, $k_w = 2\pi/\lambda_w$ is the optical wave number, λ_w is the wavelength, L is the propagation distance, and C_n^2 is the index of refraction structure parameter [14].

Pointing Error: Pointing error refers to the misalignment of the laser beam with the optical receiver, caused by i) boresight, the fixed displacement between the beam centroid and the receiver center, and ii) jitter, the random temporal displacement due to factors such as building sway, wind, or vibrations. While careful deployment or fast-tracking transmitters can minimize boresight misalignment, residual jitter remains a concern even with a well-designed ATP subsystem [11]. To account for this effect, the severity of jitter in this work is later categorized into representative regimes reflecting different levels of ATP capability (see Table I in Section IV).

After propagating a distance L , the laser beam with waist w_L is incident on the photodetector with aperture radius r_A [37]. The received optical beam attenuation due to turbulence-induced spread and pointing error, described by radial displacement r between the beam footprint and the detector center, is given by $I_p(r; L) \approx A_0 \exp(-2r^2/w_{L_{eq}}^2)$ where $w_{L_{eq}}^2 = w_L^2 \sqrt{\pi} \operatorname{erf}(v) / (2v \exp(-v^2))$ is the (squared) equivalent beam width with $v = \sqrt{\pi} r_A / \sqrt{2} w_L$. The fraction of the collected power at $r = 0$ is given by

$$A_0 = [\operatorname{erf}(v)]^2, \quad (5)$$

where $\operatorname{erf}(\cdot)$ is the standard error function [36, Eq. (8.250.1)], and $0 \leq A_0 \leq 1$ [15]. For a coherent beam, the beam radius w_L is related to the beam waist w_0 at the optical transmitter's exit aperture by $w_L = w_0(1 + \epsilon(\lambda_w L / \pi w_0^2)^2)^{1/2}$ where $\epsilon = (1 + 2w_0^2/\rho_0^2(L))$ is the global coherence parameter, $\rho_0(L) = (1.46 C_n^2 k_w^2 L)^{-3/5}$ is the coherence length in turbulence [38], and the transmit beam waist w_0 is related to the transmitter aperture diameter D as $w_0 = D/\sqrt{2}\pi$ [39]. Farid and Hranilovic [15] derived the PDF of the irradiance component I_p under the assumptions of i.i.d. zero-mean Gaussian distributions for both horizontal and vertical receiver sways (i.e., zero boresight and identical jitters), which is expressed as

$$f_{I_p}(I_p) = \frac{\xi^2}{A_0 \xi^2} I_p^{\xi^2-1}; \quad 0 \leq I_p \leq A_0 \quad (6)$$

where the parameter $\xi \triangleq w_{L_{eq}}/2\sigma_e$ is the ratio of the received equivalent beam waist $w_{L_{eq}}$ and the standard deviation of the pointing error displacement (jitter). This model is valid when $w_L/r_A \gg 1$ and further that the effects of ξ and A_0 parameters are independent [15].

A recent refinement of the pointing error model is introduced in [40], where multiple alternative parameterizations of ξ and A_0 are proposed to enhance modeling accuracy and computational efficiency (see [40, Fig. 5]). In this work, we hence borrow the *Modified Intensity Uniform Model* from [40], which retains the same mathematical form for the probability distribution as in (6), but with redefined parameters given by $A_0 = 1 - \exp(-2r_A^2/w_L^2)$ and $\xi^2 = r_A^2/(2\sigma_e^2 A_0)$. Precisely, this choice demonstrates more than an order-of-magnitude reduction in normalized mean square error (NMSE) compared to the Farid–Hranilovic formulation (see [40, Table 1]), thereby offering a substantially more reliable characterization of pointing jitter effects in terrestrial FSO links.

Composite Fading Distribution: Given the distributions in (2) and (6) of the independent constituents I_a and I_p , the PDF of the instantaneous composite irradiance $I = I_a I_p$ is developed to [25, Eq. (8)]

$$f_I(I) = \frac{ab\xi^2}{A_0\Gamma(a)\Gamma(b)} G_{1,3}^{3,0} \left(\frac{abI}{A_0} \middle| \begin{matrix} \xi^2 \\ \xi^2 - 1, a - 1, b - 1 \end{matrix} \right). \quad (7)$$

Remark 1. For longer terrestrial FSO links, and even for medium-haul links operating under strong turbulence, additional impairments such as boresight misalignment, beam wander, and angle-of-arrival fluctuations become dominant and constitute critical practical challenges. In this work, we focus on turbulence and pointing error effects, an assumption

that is well-justified for short-haul links and for medium-haul links under weak turbulence, where higher-order impairments are typically negligible or remain within acceptable limits.

B. Noise Sources in FSO Wireless Systems

Two fundamental sources of noise interfere in the process of photodetection in FSO receivers: i) the shot noise due to photodetection itself [41], and ii) the thermal noise originating in the receiver circuitry. The shot noise is due to the information optical radiation and the ambient light incident on the receiver lens, and its power grows linearly with the total incident optical power. Importantly, both ambient shot noise and thermal noise are signal-independent, as they remain statistically uncorrelated with the information-carrying optical signal [42].

The IM-DD photodetector output consists of the desirable photocurrent component mapped one-to-one to the intensity of the incoming (information) optical signal, signal-dependent shot noise, ambient shot noise, and thermal noise currents. The operating mode of the IM-DD receiver is determined by the relative strengths of these noise components, as follows.

- For an IM-DD receiver operating in intense ambient light conditions and/or strong thermal noise conditions, it is reasonable that the corrupting noise is signal-independent. It typically holds for indoor IM-DD infrared *diffuse or non-LOS* links [43].
- For the IM-DD based FSO systems with large received optical information-signal powers, it is reasonable to expect the corrupting noise to be signal-dependent [44]. It is valid for short-haul and/or medium-haul laser-based IM-DD *LOS directed* links with reasonable transmit powers [43].

In a coherent HD receiver, an optical local oscillator (OLO) signal is mixed with the received signal prior to photodetection. This introduces an OLO-dependent shot noise current in addition to signal-dependent shot noise, ambient shot noise, and thermal noise currents. By ensuring a large OLO optical power, the OLO shot noise component can be made dominant compared to other noise components; this is in fact considered to be the de facto mode of operation of an (ideal) coherent HD receiver [10], [42], [45].

Remark on the Statistical Characterization of Shot Noise: When the number of received photons per symbol interval is low—as is typical in inter-satellite and ground-to-satellite optical links—the shot noise is accurately modeled using a Poisson distribution [46]. In contrast, for high photon-count regimes, as encountered in most terrestrial FSO applications, a Gaussian approximation is sufficiently accurate. For a rigorous justification of the Gaussian model for high-intensity shot noise, refer [46], [47].

C. Receiver Models

Let $x_{\text{IMDD}} \in \mathbb{R}^+$ and $x_{\text{HD}} \in \mathbb{C}$ denote the transmitted signals for the IM-DD and coherent HD systems respectively. We remind the reader that the baseband (information) signal in a coherent HD scheme represents a complex optical field, whereas the baseband signal in an IM-DD scheme represents optical intensity. In both schemes, the transmitted beam power

is constrained by a fixed average power constraint denoted by: $\mathbb{E}[x_{\text{IMDD}}] \leq P_{\text{avg}}$ and $\mathbb{E}[|x_{\text{HD}}|^2] \leq P_{\text{avg}}$. As justified in the introduction, a frequency-flat block fading model is well-suited to capture the random irradiance fluctuations in a terrestrial optical channel: each fading state is assumed to span an identical duration, corresponding to a fixed coherence time, with i.i.d. fading realizations across blocks. The instantaneous channel state is considered to be perfectly known at both the transmitter and the receiver at all times. In practice, this state needs to be estimated only once at the beginning of each block. Within this framework, we consider a FSO transmitter that performs signal adaptation on a block-by-block basis. Adhering to this understanding, the received signal models for the two detection systems are developed next.

1) *Signal-Dependent IM-DD Receiver System:* The baseband signal in an IM-DD receiver is described by

$$y_{\text{IMDD}} = Ix_{\text{IMDD}} + \sqrt{Ix_{\text{IMDD}}}n_{\text{SD}} + n_{\text{SI}} \quad (8)$$

where y_{IMDD} is the received signal, I is the intensity fluctuation state of the terrestrial FSO link (see (7)), $n_{\text{SI}} \sim \mathcal{N}(0, \sigma_{\text{SI}}^2)$ is the signal-independent noise (combined ‘ambient and thermal noise’) modeled as additive white Gaussian noise (AWGN), and the $\sqrt{Ix_{\text{IMDD}}}n_{\text{SD}} \sim \mathcal{N}(0, Ix_{\text{IMDD}}\sigma^2)$ is the signal-dependent AWGN [44].

Remark 2. *In the signal-independent noise-limited IM-DD operation, $n_{\text{SI}} \gg \sqrt{Ix_{\text{IMDD}}}n_{\text{SD}}$ with high probability. Hence, the received SNR ($:= I^2x_{\text{IMDD}}^2/\sigma_{\text{SI}}^2$) varies as the ‘square’ of the received optical power. In [25], [26], [27], the average SE maximization problem for the signal-independent noise-limited IM-DD channel is formulated as $\mathbb{E}[\ln(1 + I^2P^2(I))]$ where $P^2(I) := x_{\text{IMDD}}^2$ under the constraint $\mathbb{E}[P(I)] = P_{\text{avg}}$; this is a non-convex optimization, and more seriously, the above SE formulation ignored the non-negativity constraint on I (see [48] for details).*

In this work, we consider the signal-dependent noise-limited IM-DD receiver; thus, the noise power is dominated by $Ix_{\text{IMDD}}\sigma^2$. Hence, conditioned on I , the received SNR is

$$\gamma_{\text{IMDD}} = Ix_{\text{IMDD}}/\sigma^2. \quad (9)$$

Notice from (9) that the SNR varies *linearly* with the incident optical power at the considered IM-DD receiver.

2) *Coherent Heterodyne Detection Receiver System:* The complex baseband signal in a coherent HD receiver is given by

$$y_{\text{HD}} = hx_{\text{HD}} + w_{\text{OLO}} + w_{\text{OTH}} \quad (10)$$

where $y_{\text{HD}} \in \mathbb{C}$ represents its output, $h \in \mathbb{C}$ the fluctuation in the received optical field, $w_{\text{OLO}} \sim \mathcal{CN}(0, \sigma_{\text{OLO}}^2)$ the OLO shot noise, and w_{OTH} the total AWGN from all the sources other than the OLO [13, Ch. 3]. The OLO shot noise is the only dominant noise of consequence. Hence, conditioned on h or more appropriately on $I := |h|^2$, the received SNR is

$$\gamma_{\text{HD}} = I|x_{\text{HD}}|^2/\sigma_{\text{OLO}}^2. \quad (11)$$

III. ACHIEVABLE SPECTRAL EFFICIENCY WITH ADAPTIVE OPTICAL BEAM TRANSMISSION

The transmitted signal x_{IMDD} , representing optical intensity, must be non-negative. In contrast, the x_{HD} scheme has no

such constraint and can utilize two degrees of freedom. As a result, the classical Shannon limit on spectral efficiency for the AWGN channel applies to the HD scheme, but not to the IM-DD system (see [48]). Conditioned on the received SNRs in (9) and (11), the SE of the optical channels (expressed in nats/s/Hz) based on IM-DD and HD schemes satisfy

$$S_{\text{IMDD}}(I) \geq \frac{1}{2} \ln \left(1 + \frac{\gamma_E}{2\pi} \frac{I x_{\text{IMDD}}}{\sigma^2} \right), \quad (12)$$

$$S_{\text{HD}}(I) = \ln \left(1 + \frac{I |x_{\text{HD}}|^2}{\sigma_{\text{OLO}}^2} \right). \quad (13)$$

In (12), the constant γ_E is the Euler's constant. The lower bound on the achievable SE of the signal-dependent IM-DD channel, given by (12), is derived from [48, Theorem 7] for the AWGN IM-DD channel under an average-power constraint. This bound approaches the actual SE at high received optical powers [48, Proposition 8], making it a reliable approximation in such regimes. Using (12) and (13), a unified SE expression for a given channel state $\lambda := I$ can be derived for both FSO systems as follows.

$$S(\lambda) := \frac{1}{k} \ln \left(1 + \frac{\lambda P_k(\lambda)}{N_k} \right) \quad (14)$$

where $k = 1$ for the HD based scheme with $N_1 = \sigma_{\text{OLO}}^2$, $P_1(\lambda) := |x_{\text{HD}}|^2$, and $k = 2$ for the IM-DD based scheme with $N_2 = \sigma^2/(\gamma_E/2\pi)$, $P_2(\lambda) := x_{\text{IMDD}}$. The power constraint mentioned earlier for both schemes gets translated to $\mathbb{E}[P_k(\lambda)] \leq P_{\text{avg}}$.

The average (long-term) spectral efficiency (ASE) in nats/s/Hz is given by

$$\bar{S} = \max_{P_k} \frac{1}{k} \mathbb{E} \left[\ln \left(1 + \frac{\lambda P_k(\lambda)}{N_k} \right) \right] \quad (15)$$

where the maximization is performed over all feasible transmit laser beam adaptation schemes that satisfy $\mathbb{E}[P_k(\lambda)] \leq P_{\text{avg}}$.

Note that P_{avg}/N_k represents the average transmit power normalized by the average noise power, which will henceforth be termed the *transmit SNR* and denoted by SNR_k . The optimal beam power adaptation P_k^* maximizing (15) is

$$\frac{P_k^*(\lambda)}{N_k} = \left(\frac{1}{\mu_k} - \frac{1}{\lambda} \right)^+ \quad (16)$$

with μ_k chosen so that the optical power constraint

$$\mathbb{E} \left[\left(\frac{1}{\mu_k} - \frac{1}{\lambda} \right)^+ \right] = \text{SNR}_k \quad (17)$$

is satisfied. Additionally, the parameter μ_k serves as a channel cutoff, which simplifies the ASE problem in (15) to

$$\bar{S} = \frac{1}{k} \int_{\mu_k}^{\infty} \ln \left(\frac{\lambda}{\mu_k} \right) f_{\lambda}(\lambda) d\lambda. \quad (18)$$

To compute \bar{S} , we divide the integral in (18) into three parts as follows.

$$\bar{S} = \frac{1}{k} \left[\underbrace{\int_0^{\infty} \ln(\lambda) f_{\lambda}(\lambda) d\lambda}_{=I_1} - \underbrace{\int_0^{\mu_k} \ln(\lambda) f_{\lambda}(\lambda) d\lambda}_{=I_2} - \underbrace{\int_{\mu_k}^{\infty} \ln(\mu_k) f_{\lambda}(\lambda) d\lambda}_{=I_3} \right]. \quad (19)$$

In evaluating the integrals I_1 , I_2 and I_3 , we will frequently apply an integral identity involving the Meijer-G function [36, Eq. (9.301)], which is reproduced below (see [49] for additional details).

$$\int x^{j-1} G_{p,q}^{m,n} \left(x \left| \begin{matrix} a_1, \dots, a_p \\ b_1, \dots, b_q \end{matrix} \right. \right) dx = G_{p+1,q+1}^{m,n+1} \left(x \left| \begin{matrix} 1, j+a_1, \dots, j+a_n, j+a_{n+1}, \dots, j+a_p \\ j+b_1, \dots, j+b_m, 0, j+b_{m+1}, \dots, j+b_q \end{matrix} \right. \right). \quad (20)$$

A. Exact ASE With and Without Pointing Errors

Theorem 1. For the GG turbulence channel with pointing error and perfect channel state information (CSI) at both ends, the exact ASE is given by

$$\bar{S} = \frac{1}{k} \left[\ln \left(\frac{A_0}{ab} \right) + \psi(a) + \psi(b) - \ln(\mu_k) - \left(\frac{1}{\xi^2} \right) + \frac{\xi^2}{\Gamma(a)\Gamma(b)} G_{3,5}^{3,2} \left(\frac{ab}{A_0} \mu_k \left| \begin{matrix} 1, 1, \xi^2 + 1 \\ \xi^2, a, b, 0, 0 \end{matrix} \right. \right) \right] \quad (21)$$

where $\psi(\cdot)$ is the Euler's digamma function, and μ_k is determined from $\int_{\mu_k}^{\infty} (1/\mu_k - 1/\lambda) f_{\lambda}(\lambda) d\lambda = \text{SNR}_k$.

Proof: The unified ASE expression (from (19)) is

$$\bar{S} = (I_1 - I_2 - I_3)/k. \quad (22)$$

Evaluation of Integral I_1 : The integral I_1 can be viewed as

$$I_1 = \mathbb{E} [\ln \lambda]. \quad (23)$$

We reformulate (23) by taking expectation on the identity $\frac{d}{dt} \lambda^t = \lambda^t \ln(\lambda)$ and thereupon evaluating at $t = 0$ such that

$$\mathbb{E} [\lambda^t \ln(\lambda)] \Big|_{t=0} = \frac{d}{dt} (\mathbb{E} [\lambda^t]) \Big|_{t=0}$$

and hence $I_1 = \frac{d}{dt} \left(\int_0^{\infty} \lambda^t f_{\lambda}(\lambda) d\lambda \right) \Big|_{t=0}$. (24)

The t -th moment in the RHS of (24) is computed as

$$\int_0^{\infty} \lambda^t f_{\lambda}(\lambda) d\lambda = \frac{ab\xi^2}{A_0\Gamma(a)\Gamma(b)} \int_0^{\infty} \lambda^t G_{1,3}^{3,0} \left(\frac{ab\lambda}{A_0} \left| \begin{matrix} \xi^2 \\ \xi^2 - 1, a - 1, b - 1 \end{matrix} \right. \right) d\lambda. \quad (25)$$

Applying (20) in (25) along with the substitutions that

$$\lim_{x \rightarrow 0} G_{2,4}^{3,1} \left(x \left| \begin{matrix} 1, \xi^2 + t + 1 \\ \xi^2 + t, a + t, b + t, 0 \end{matrix} \right. \right) = 0, \text{ and}$$

$$\lim_{x \rightarrow \infty} G_{2,4}^{3,1} \left(x \left| \begin{matrix} 1, \xi^2 + t + 1 \\ \xi^2 + t, a + t, b + t, 0 \end{matrix} \right. \right) = \frac{\Gamma(a+t)\Gamma(b+t)}{\xi^2 + t},$$

we have

$$I_1 = \frac{\xi^2}{\Gamma(a)\Gamma(b)} \frac{d}{dt} \left(\left(\frac{A_0}{ab} \right)^t \frac{\Gamma(a+t)\Gamma(b+t)}{\xi^2+t} \right) \Big|_{t=0}. \quad (26)$$

Upon differentiation w.r.t. t and then evaluating the attained expression for $t = 0$, we obtain the final I_1 expression as

$$I_1 = \ln\left(\frac{A_0}{ab}\right) + \psi(a) + \psi(b) - \left(\frac{1}{\xi^2}\right). \quad (27)$$

In the above, we have used $d(\ln\Gamma(x))/dx = \psi(x)$.

Evaluation of Integral I_2 : The integral part I_2 is now evaluated as

$$\begin{aligned} I_2 &= \int_0^{\mu_k} \ln(\lambda) f_\lambda(\lambda) d\lambda \\ &= \frac{ab\xi^2}{A_0\Gamma(a)\Gamma(b)} \int_0^{\mu_k} \ln(\lambda) G_{1,3}^{3,0} \left(\frac{ab\lambda}{A_0} \middle| \xi^2 - 1, a - 1, b - 1 \right) d\lambda. \end{aligned}$$

We apply the integration-by-parts technique treating $\ln(\cdot)$ as the first function and the Meijer-G function as the second to get

$$\begin{aligned} I_2 &= \left[G_{2,4}^{3,1} \left(\frac{ab\lambda}{A_0} \middle| 1, \xi^2 + 1 \right) \times \ln(\lambda) \right. \\ &\quad \left. - G_{3,5}^{3,2} \left(\frac{ab\lambda}{A_0} \middle| 1, 1, \xi^2 + 1 \right) \right] \Big|_{\lambda=0}^{\lambda=\mu_k} \times \frac{\xi^2}{\Gamma(a)\Gamma(b)}. \quad (28) \end{aligned}$$

With the Meijer-G function limits

$$\begin{aligned} \lim_{x \rightarrow 0} G_{2,4}^{3,1} \left(x \middle| 1, \xi^2 + 1 \right) \times \ln(x) &= 0, \text{ and} \\ \lim_{x \rightarrow 0} G_{3,5}^{3,2} \left(x \middle| 1, 1, \xi^2 + 1 \right) &= 0, \end{aligned}$$

the final I_2 expression is given by

$$\begin{aligned} I_2 &= \left[G_{2,4}^{3,1} \left(\frac{ab}{A_0} \mu_k \middle| 1, \xi^2 + 1 \right) \times \ln(\mu_k) \right. \\ &\quad \left. - G_{3,5}^{3,2} \left(\frac{ab}{A_0} \mu_k \middle| 1, 1, \xi^2 + 1 \right) \right] \frac{\xi^2}{\Gamma(a)\Gamma(b)}. \quad (29) \end{aligned}$$

Evaluation of Integral I_3 : The I_3 component is given as

$$I_3 = \ln(\mu_k) \int_{\mu_k}^{\infty} f_\lambda(\lambda) d\lambda, \quad (30)$$

where the integral is computed as

$$\begin{aligned} &\int_{\mu_k}^{\infty} f_\lambda(\lambda) d\lambda \\ &= 1 - \frac{ab\xi^2}{A_0\Gamma(a)\Gamma(b)} \int_0^{\mu_k} G_{1,3}^{3,0} \left(\frac{ab\lambda}{A_0} \middle| \xi^2 - 1, a - 1, b - 1 \right) d\lambda \\ &= 1 - \frac{\xi^2}{\Gamma(a)\Gamma(b)} G_{2,4}^{3,1} \left(\frac{ab}{A_0} \mu_k \middle| 1, \xi^2 + 1 \right). \quad (31) \end{aligned}$$

The last equality is obtained by applying the identity in (20) along with the substitution that

$$\lim_{x \rightarrow 0} G_{2,4}^{3,1} \left(x \middle| 1, \xi^2 + 1 \right) = 0.$$

Substituting these I_1, I_2 and I_3 expressions back into (22) and consequent simplification gives the final closed-form expression of the ASE in Theorem 1. ■

The ASE with dynamic beam power adaptation over the GG turbulence channel (but without pointing error) is a useful baseline for comparison as follows.

Corollary 1. *For the GG turbulence channel ‘without pointing error’ and perfect CSI at both ends, the exact ASE is given by*

$$\begin{aligned} \bar{S} &= \frac{1}{k} \left[\ln\left(\frac{1}{ab}\right) + \psi(a) + \psi(b) - \ln(\mu_k) \right. \\ &\quad \left. + \frac{1}{\Gamma(a)\Gamma(b)} G_{2,4}^{2,2} \left(ab\mu_k \middle| 1, 1 \right) \right] \quad (32) \end{aligned}$$

where μ_k is solved from $\int_{\mu_k}^{\infty} (1/\mu_k - 1/\lambda) f_\lambda(\lambda) d\lambda = \text{SNR}_k$.

Proof: In the limiting case where $A_0 \rightarrow 1$ and $\xi^2 \rightarrow \infty$, the fading distribution converges to the pure GG distribution. Substituting these limits into (21) and applying the identity from [36, Eq. (9.31.1)] completes the proof of the theorem. ■

To the best of the authors’ knowledge, the proposed exact ASE solutions, Theorems 1 and Corollary 1, for the GG turbulence channels with and without pointing error are new.

B. Immediate Insights

The proposed ASE formula is interesting in obtaining quantitative as well as qualitative insights as follows.

- At high SNRs, contribution from the Meijer-G based term vanishes while $\mu_k \rightarrow 1/\text{SNR}_k$. Keeping this in mind, and now comparing the ASE of channels with and without pointing error, the ASE loss due to pointing error can be easily quantified in terms of A_0 and ξ^2 parameters.
- Likewise, the ASE loss due to both turbulence and pointing error at high SNR when compared with no channel impairments (pure AWGN) can also be quantified and analyzed.
- In a fixed terrestrial FSO link, variation in turbulence can lead to change in the pointing error behavior. In such a scenario, the derived closed-form ASE expression also allows an accurate analysis of the impact of these interlinked channel parameters.

A more in-depth and broader exposition of adaptive transmission benefits and the impact of channel impairments will be presented in Section IV, allowing for a wide range of variations in channel turbulence, pointing error, and SNR.

C. Low-SNR and High-SNR Asymptotic Expressions

The asymptotic expansions of the exact ASE expression reveal how key channel parameters from GG turbulence and pointing error influence the performance of adaptive FSO schemes. To this end, the μ_k -SNR $_k$ relationship is first derived under average power constraint in both low-SNR and high-SNR regimes.

Lemma 1. *The threshold value μ_k associated with the optimal beam power adaptation as described in (16) for the transmitted laser beam satisfies*

- 1) *At high SNR:* $\mu_k \approx \frac{1}{\text{SNR}_k}$,
- 2) *At low SNR:* $\mu_k \approx \frac{A_0}{4ab} \ln^2\left(\frac{1}{\text{SNR}_k}\right)$.

Proof: Part 1): Substituting (7) into the average optical power constraint (17), we have

$$\frac{\mu_k \text{SNR}_k}{A} = \int_{\mu_k}^{\infty} \left(1 - \frac{\mu_k}{\lambda}\right) G_{1,3}^{3,0} \left(\frac{ab\lambda}{A_0} \middle| \begin{matrix} \xi^2 \\ \xi^2 - 1, a - 1, b - 1 \end{matrix} \right) d\lambda,$$

where $A = ab\xi^2/(A_0\Gamma(a)\Gamma(b))$. Applying the identity in (20) to the power constraint equation gives

$$\begin{aligned} \frac{\mu_k \text{SNR}_k}{A} &= \frac{1}{A} - \frac{A_0}{ab} G_{2,4}^{3,1} \left(\frac{ab}{A_0} \mu_k \middle| \begin{matrix} 1, \xi^2 + 1 \\ \xi^2, a, b, 0 \end{matrix} \right) \\ &+ \mu_k G_{2,4}^{3,1} \left(\frac{ab}{A_0} \mu_k \middle| \begin{matrix} 1, \xi^2 \\ \xi^2 - 1, a - 1, b - 1, 0 \end{matrix} \right). \end{aligned} \quad (33)$$

From the power constraint in (17), it follows that μ_k exhibits a strictly monotonic inverse relation with SNR_k , decreasing as SNR_k increases. Notably, at high SNRs, the contributions of the Meijer-G function terms in (33) become negligible due to their vanishing behavior for small arguments. Hence

$$\lim_{\mu_k \rightarrow 0} \mu_k \text{SNR}_k = 1.$$

This completes the proof of 1).

Part 2): We now derive an explicit expression for the μ_k - SNR_k dependence in the low-SNR regime. As SNR_k decreases, the cutoff μ_k increases, leading the transmitter to allocate power only for high channel gains. To facilitate this, the channel gain distribution $f_\lambda(\lambda)$ in (7) is approximated using a low-order series expansion of the Meijer G-function for large arguments, as detailed below:

$$G_{1,3}^{3,0} \left(z \middle| \begin{matrix} \xi^2 \\ \xi^2 - 1, a - 1, b - 1 \end{matrix} \right) \approx e^{-2\sqrt{z}} \sqrt{\pi} z^{\frac{1}{4}(-7+2a+2b)}. \quad (34)$$

Only the dominant term of the series expansion is shown in (34), and substituting it into the LHS of the constraint (17) yields

$$\text{SNR}_k \approx K \left(\frac{B_1(ab\mu_k/A_0)}{ab\mu_k/A_0} - B_2(ab\mu_k/A_0) \right) \quad (35)$$

where $K = (\sqrt{\pi} ab \xi^2)/(A_0\Gamma(a)\Gamma(b))$ is a positive constant independent of the threshold value, and

$$B_1(x) := 2^{-n} \Gamma(n+1, 2\sqrt{x}), \quad (36)$$

$$B_2(x) := 2^{2-n} \Gamma(n-1, 2\sqrt{x}), \quad (37)$$

where, in turn, $n := a + b - \frac{5}{2}$, and $\Gamma(\cdot, \cdot)$ denotes the upper incomplete Gamma function, whose large-argument series expansion is given below [36]:

$$\Gamma(s, t) \approx t^s e^{-t} \left(\frac{1}{t} + \frac{s-1}{t^2} + o\left(\frac{1}{t}\right)^3 \right). \quad (38)$$

By retaining the two leading terms in (38), (35) simplifies to

$$\text{SNR}_k \approx K \left(\frac{ab}{A_0} \mu_k \right)^{\left(\frac{a+b}{2} - \frac{11}{4}\right)} e^{-2\sqrt{\frac{ab}{A_0} \mu_k}}. \quad (39)$$

Taking the logarithm of both sides of (39) and retaining the dominant term on the right-hand side, we obtain

$$\ln(\text{SNR}_k) \approx -2\sqrt{ab\mu_k/A_0}. \quad (40)$$

Solving (40) for μ_k , we finally arrive at

$$\mu_k \approx \frac{A_0}{4ab} \ln^2 \left(\frac{1}{\text{SNR}_k} \right). \quad (41)$$

This completes the proof of 2). ■

Theorem 2. For the GG turbulence channel with pointing error, the asymptotic ASE at low and high SNR are given by

$$\bar{S}_{low} \approx \frac{1}{k} \left[\frac{A_0}{4ab} \text{SNR}_k \ln^2 \left(\frac{1}{\text{SNR}_k} \right) \right], \quad \text{and} \quad (42)$$

$$\bar{S}_{high} \approx \frac{1}{k} \left[\ln \text{SNR}_k + \ln \left(\frac{A_0}{ab} \right) + \psi(a) + \psi(b) - \left(\frac{1}{\xi^2} \right) \right] \quad (43)$$

where the subscripts ‘low’ and ‘high’ stand for the low-SNR (asymptotically 0) and high-SNR (asymptotically ∞) regimes respectively.

Proof: Part 1): At high SNR, the threshold behaves as $\mu_k \approx \text{SNR}_k^{-1}$ (from Lemma 1), while the Meijer’s G function becomes negligible for small input arguments, asymptotically approaching zero as

$$\lim_{z \rightarrow 0} G_{3,5}^{3,2} \left(z \middle| \begin{matrix} 1, 1, \xi^2 + 1 \\ \xi^2, a, b, 0, 0 \end{matrix} \right) = 0. \quad (44)$$

With these substitutions in Theorem 1, (43) is proved.

Part 2): The low-order series expansion of the Meijer-G function in (21) for large input argument z (asymptotically ∞) is

$$\begin{aligned} G_{3,5}^{3,2} \left(z \middle| \begin{matrix} 1, 1, \xi^2 + 1 \\ \xi^2, a, b, 0, 0 \end{matrix} \right) &\approx e^{-2\sqrt{z}} \sqrt{\pi} z^{\frac{1}{4}(-7+2a+2b)} \\ &+ \frac{\Gamma(a)\Gamma(b)}{\xi^2} \left(\ln(z) + \frac{1}{\xi^2} - \psi(a) - \psi(b) \right). \end{aligned} \quad (45)$$

Substituting the above series expansion in (21), we observe

$$\bar{S} \approx \frac{K}{k(ab/A_0)} \left(\frac{ab}{A_0} \mu_k \right)^{\left(\frac{a+b}{2} - \frac{7}{4}\right)} e^{-2\sqrt{\frac{ab}{A_0} \mu_k}}. \quad (46)$$

Comparing (46) with (39) derived in connection with the lemma 1, we find that

$$\bar{S} \approx \frac{\mu_k \text{SNR}_k}{k}. \quad (47)$$

Finally, substituting μ_k from (41) in (47) completes the proof of the low SNR ASE expansion (42) in Theorem 2. ■

A few interesting observations from the derived theorems are as follows.

- By applying $A_0 \rightarrow 1$ and $\xi^2 \rightarrow \infty$, the asymptotic ASEs of the GG turbulence channel ‘without pointing error’ at low and high SNR are computed as

$$\bar{S}_{low} \approx \frac{1}{k} \left[\frac{1}{4ab} \text{SNR}_k \ln^2 \left(\frac{1}{\text{SNR}_k} \right) \right], \quad \text{and} \quad (48)$$

$$\bar{S}_{high} \approx \frac{1}{k} \left[\ln \text{SNR}_k + \ln \left(\frac{1}{ab} \right) + \psi(a) + \psi(b) \right]. \quad (49)$$

- By comparing (43) and (49), a measure of the ASE degradation due to pointing errors at high SNRs can be found as

$$\frac{1}{k} \left[\frac{1}{\xi^2} - \ln A_0 \right]. \quad (50)$$

- For the GG turbulence channel, the presence of pointing errors decreases the ASE at low SNRs by A_0 times.

The derived asymptotic results in (42), (43), (48) and (49) are useful for a comprehensive assessment of the impact of variations of turbulence and pointing error statistics over a wide range.

IV. NUMERICAL RESULTS AND DISCUSSION

In this section, we present the analytical utility of the derived ASE formulas, supported by extensive numerical results. Previous studies on related topics [25], [28], [29], [31], and [32] have suggested, both directly and indirectly, that a wide range of optical turbulence conditions can be achieved by varying the FSO link length. However, link length variations impact the large-scale path loss factor. Additionally, the laser beam waist expands with propagation distance, impacting the pointing error distribution parameters ξ and A_0 . Notably, these studies did not consider these interdependencies. Understanding the interactions among these channel characteristics is essential, as this work aims to accurately analyze the impact of variations in turbulence and pointing error on the ASE performance of terrestrial FSO systems.

TABLE I
FSO SYSTEM AND CHANNEL SETTINGS

Parameter	Symbol	Value
Optical wavelength	λ_w	1550 nm
Beam waist (at Tx.)	w_0	0.45 cm
FSO channel length	L	300 m
Rx. Aperture radius	r_A	1 cm
Tx./Rx. optics eff.	–	100% (assumed)
Path loss factor	–	Unity (assumed)

Ch. Setting (a): Gamma-Gamma (GG) fading ‘without’ pointing error		
Turbulence strength	Rytov variance σ_R^2	GG distribution parameters
Weak	0.2	$a = 11.651, b = 10.122$
Moderate	1	$a = 4.3939, b = 2.5636$
Strong	4	$a = 4.3407, b = 1.3088$

Ch. Setting (b): GG fading with ‘mild’ pointing error ($\sigma_e = 1$ cm)		
Turbulence strength	Rytov variance σ_R^2	Pointing Error distribution parameters
Weak	0.2	$\xi = 1.8102, A_0 = 0.1526$
Moderate	1	$\xi = 2.1977, A_0 = 0.1035$
Strong	4	$\xi = 3.5510, A_0 = 0.0397$

Ch. Setting (c): GG fading with ‘strong’ pointing error ($\sigma_e = 4$ cm)		
Turbulence strength	Rytov variance σ_R^2	Pointing Error distribution parameters
Weak	0.2	$\xi = 0.4525, A_0 = 0.1526$
Moderate	1	$\xi = 0.5494, A_0 = 0.1035$
Strong	4	$\xi = 0.8877, A_0 = 0.0397$

To ensure a fair comparison, the FSO Tx-Rx system parameters (e.g., optical wavelength, Tx. beam waist, Rx. aperture) are kept fixed. In addition, a horizontal terrestrial FSO link of ‘fixed length’ is considered, ensuring that the path loss factor remains unchanged. A horizontal distance of 300 m, representative of short-to-medium haul FSO links, is selected to capture realistic turbulence and pointing error effects while keeping other impairments negligible (see Remark 1). To

explicitly account for the acquisition, tracking, and pointing (ATP) subsystem, three representative GG channel settings are considered: (a) *No pointing error*, corresponding to an ideal or “genie-aided” ATP subsystem that fully eliminates jitter, serving as a turbulence-limited benchmark; (b) *Mild pointing error*, corresponding to a realistic, well-designed ATP subsystem with small residual jitter; and (c) *Strong pointing error*, corresponding to a poorly designed or absent ATP subsystem (i.e., no ATP), where jitter dominates. Although such severe jitter exceeds typical values observed in practical systems with ATP, it is included for theoretical completeness, highlighting the transition from turbulence-limited to jitter-dominated operation.

These settings cover the practical range of ATP capabilities and provide a unified framework for analyzing turbulence-limited, jitter-limited, and intermediate regimes.

To span a realistic weak-to-strong turbulence range while maintaining constant path loss, we recall that the turbulence strength is governed by the Rytov variance

$$\sigma_R^2 = 1.23 C_n^2 k_w^{7/6} L^{11/6} \quad (51)$$

which underscores its dependence on the index of refraction structure parameter C_n^2 , as discussed below.

Remark 3. For near-ground horizontal propagation, the parameter C_n^2 remains relatively constant and primarily varies with altitude—being stronger near the ground and weaker at higher elevations [11, Sec. 12.2], [50, Ch. 2].

A few additional important considerations to be noted before proceeding with the numerical results.

- Recall from (16) and (17) that $\text{SNR} := P_{\text{avg}}/N_0$ is the average transmit SNR in all the derived ASE formulae (with subscript k now suppressed from the SNR symbol as the noise levels are assumed the same) and that the horizontal axis in Figures 1–7 is the transmit SNR in log scale, not the received SNR. This enables fair comparison and accurate analysis mentioned earlier. If required, the average received SNR can be computed by scaling the transmit SNR by the mean channel gain $\mathbb{E}[\lambda]$.
- All ASE values (bits/sec/Hz is the unit of measurement) are plotted by scaling the derived expressions by $1/(\ln 2)$.
- As discussed in the introduction, a fundamental distinction between the two FSO wireless systems, namely IM-DD and coherent HD-based communication systems, lies in their noise characteristics [10]. For the same transmit SNR, the received SNR after photodetection is typically higher with a coherent receiver than with an IM-DD receiver. For analytical consistency and concreteness, we assume that the noise power levels (per Hz) in both detection receivers are the same, $N_1 = N_2 = N_0$ say.

1) *Exact ASE behavior:* Based on Theorem 1, the exact ASE for HD and IM-DD optical channels under GG turbulence, with and without pointing errors, is computed and shown in Figures 1 and 2, respectively. The analytical results closely match Monte Carlo simulation outcomes across a wide SNR range and under various turbulence strengths and pointing jitter conditions.

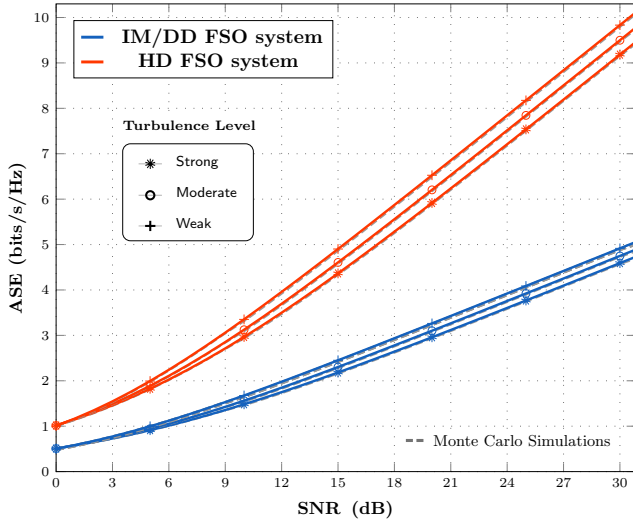


Fig. 1. Average spectral efficiency of the GG turbulence channel without pointing error under HD and IM-DD detection schemes. The average received SNR is the same as the transmit SNR since the mean channel gain $\mathbb{E}[\lambda] = 1$.

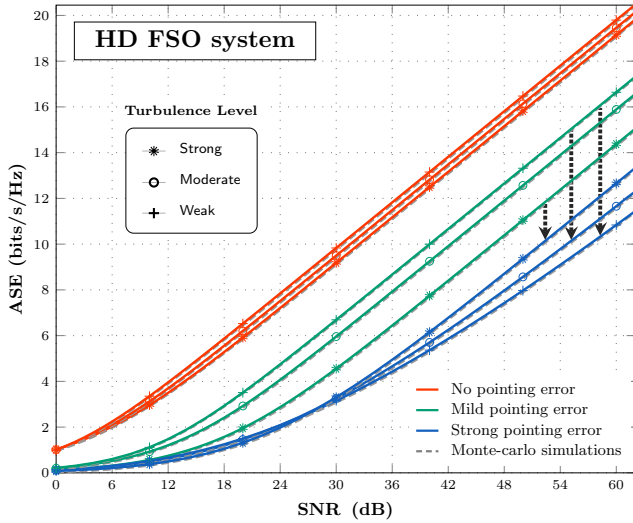


Fig. 2. Average spectral efficiency of the GG turbulence channel with pointing jitter under coherent HD detection scheme. The received SNR is less than the transmit SNR by the mean channel gain $\mathbb{E}[\lambda]$.

Discussion: Figures 1 and 2 provide the following key observations:

- As shown in Fig. 1, spectral efficiency deteriorates with increasing turbulence at high SNR for both detection schemes. This is expected, as stronger turbulence leads to a heavier concentration of low channel gains in the PDF (cf. Fig. 6).
- As shown in Fig. 2, a significant drop in spectral efficiency at high SNRs is observed in the presence of pointing errors. This is due to the effective SNR reduction at the receiver by the factor $\mathbb{E}[\lambda]$: milder jitter levels result in a moderate reduction in effective SNR, while severe jitter leads to a significant degradation in system performance.
- Interestingly, Fig. 2 reveals that, under strong pointing errors, spectral efficiency improves with turbulence in the high-SNR regime: the transition from ASE degradation to improvement initiates at transmit SNR of 30 dB, and correspondingly to a received SNR of $(30 - 17.58) \approx 12.42$ dB

(since $\mathbb{E}[\lambda] = -17.58$ dB). To explain this counterintuitive behavior, an asymptotic high-SNR analysis is carried out next.

2) *ASE behavior at High SNRs:* The high-SNR asymptotic ASE behavior in (43), as established in Theorem 2, invites comparison with the ASE of an ideal AWGN channel, which is asymptotically given by $\ln \text{SNR}$. The resulting difference—being strictly negative—quantifies the *spectral efficiency loss* at high SNRs due to the combined impairments of GG turbulence and pointing jitter, i.e.,

$$\bar{S}_{\text{penalty}} \triangleq \ln \left(\frac{A_0}{ab} \right) + \psi(a) + \psi(b) - \left(\frac{1}{\xi^2} \right). \quad (52)$$

Discussion: Fig. 3 illustrates the spectral efficiency penalty (52) plotted as a function of atmospheric turbulence strength for mild and strong pointer error channel settings (see Table I). Recall that a fixed-length horizontal FSO link is considered, with a laser beam of waist $w_0 = 4.5$ mm at the transmitter (see Table I). The beam footprint at the receiver is broadened due to beam divergence caused by turbulence over the link length. For the strong pointing error channel setting, the enlarged beam footprint leads to

- a reduction in collected power at the fixed-aperture receiver (i.e., decreased A_0); and
- a possible mitigation of the pointing jitter effect (i.e., increased ξ).

As shown in Fig. 3, for the GG fading with strong pointing error channel setting, the ASE at high SNR increases with turbulence in the practical $0 < \sigma_R^2 \leq 4$ range. This ASE behavior arises because the reduction in the pointing jitter effect more than compensates for the loss in collected power at the receiver. Consequently, the ASE penalty spans approximately -10 to -7.1 bits/s/Hz, indicating a remarkable improvement of nearly 3.0 bits/s/Hz in the high SNR regime.

For the GG fading with mild pointing error channel setting, no such trade-off is observed, as ξ exhibits negligible

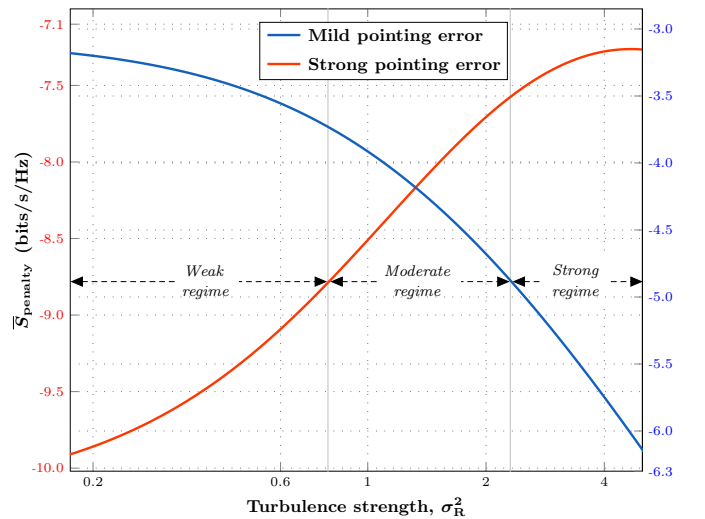


Fig. 3. The loss in average spectral efficiency at high SNRs as a function of turbulence strength for the GG channel with pointing jitter under HD detection scheme.

turbulence-induced gain while A_0 continues to decay, leading to a monotonic ASE loss. The corresponding high-SNR penalty, illustrated by the blue curve in Fig. 3, ranges from -3.2 to -6.1 bits/s/Hz.

In the GG fading without pointing error, on the other hand, the penalty at high SNRs is described by (see (49))

$$\bar{S}_{\text{penalty}} = \psi(a) + \psi(b) - \ln(ab) \quad (53)$$

which corresponds to a relatively small reduction, as can be inferred from Fig. 2 (further qualification in Fig. 4 below).

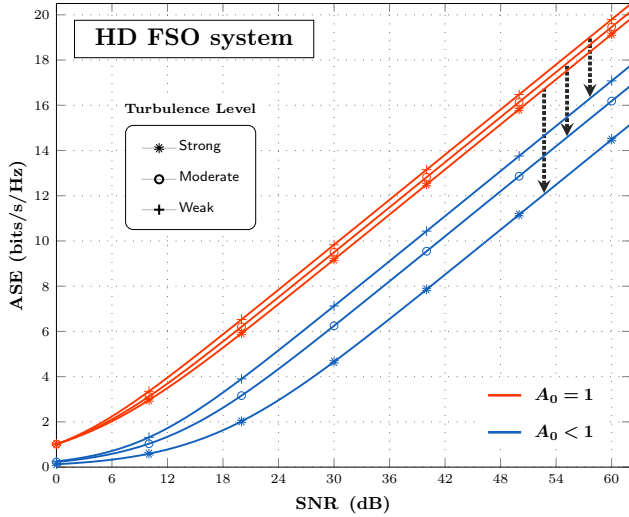


Fig. 4. Average spectral efficiency of the GG turbulence channel "without" pointing error under HD scheme: $A_0 = 1$ for "ideal" system condition whereas A_0 from Table I are considered as representation for realistic system condition.

Two additional observations can be drawn from the ASE results as follows.

- A common inconsistency in the literature is the omission of the parameter A_0 when modeling optical fading without pointing errors. While $A_0 = 1$ is often assumed for simplicity, practical FSO systems may exhibit $A_0 < 1$ due to beam divergence and finite aperture effects. Both cases are realistic in practice, but neglecting $A_0 < 1$, when not physically justified, can lead to an overestimated performance, as illustrated in Fig. 4.
- From Fig. 4, the degradation in ASE due to varying turbulence (weak to strong) under the $A_0 = 1$ condition is modest at only 0.5 bits/s/Hz. In contrast, when $A_0 < 1$, the ASE degradation due to turbulence increases significantly to 2.6 bits/s/Hz. This contrast highlights the importance of modeling A_0 accurately. The vertical downward-pointing arrows in Fig. 4 further indicate that the ASE reduction associated with $A_0 < 1$ is more severe under strong turbulence and less pronounced under weak turbulence.
- For the *fixed-length* optical channel with a constant FSO system configuration, as considered here, an important observation arises regarding the impact of increasing pointing jitter. Recall that σ_e represents the standard deviation of the pointing jitter. At high SNR, the corresponding ASE

degradation (in nats/s/Hz) attributable solely to jitter can be obtained directly from (43) and is expressed as

$$\bar{S}_{\text{loss}}^{\Delta\xi} \approx \frac{1}{k} \left[\frac{1}{\xi_{\text{new}}^2} - \frac{1}{\xi_{\text{old}}^2} \right] = \frac{4(\sigma_{e,\text{new}}^2 - \sigma_{e,\text{old}}^2)}{k w_{L_{\text{eq}}}^2} \quad (54)$$

where $w_{L_{\text{eq}}}$ denotes the received equivalent beam waist (see just above Eq. (5)). As turbulence intensity increases, $w_{L_{\text{eq}}}$ also increases, and vice versa. Hence, the ASE loss associated with a given increment in pointing jitter exhibits an inverse dependence on turbulence strength: the penalty is reduced under stronger turbulence fluctuations and amplified under weaker fluctuations, as illustrated by the vertical down-arrowed lines in Fig. 2.

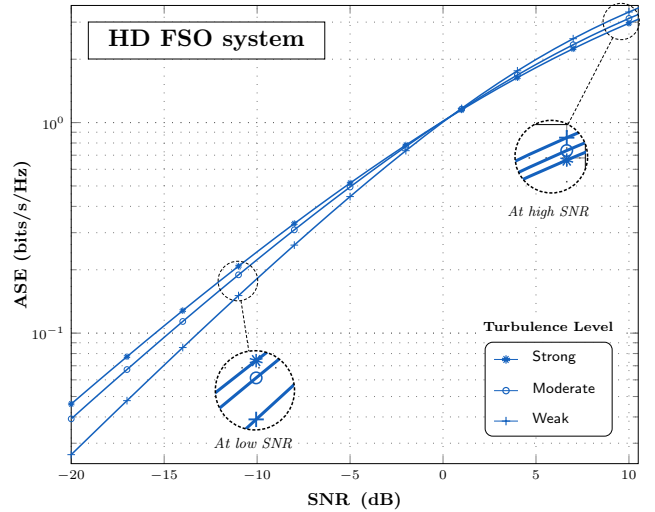


Fig. 5. Spectral efficiency at low SNRs for the GG turbulence channel without pointing jitter under HD detection scheme (see Table I for turbulence settings).

3) *Exact and asymptotic ASE behavior at Low SNRs:* As highlighted in the introduction, understanding the ASE limit of terrestrial FSO links at low SNRs is of practical interest. At low power budgets, power control of the transmitted laser beam becomes critical, requiring efficient exploitation of channel fading.

Discussion: Fig. 5 presents the exact ASE for the GG fading channel without pointing error under the HD detection scheme at low SNRs. Somewhat surprisingly, the low-SNR spectral efficiency improves with increasing turbulence. This agrees with (48), which shows that strengthening GG turbulence from profile (a_i, b_i) to (a_j, b_j) yields the following ASE improvement factor at sufficiently low SNRs:

$$\text{ASE improvement factor} \approx \frac{a_j b_j}{a_i b_i}. \quad (55)$$

This ASE improvement with turbulence at low SNRs is attributed to the enhanced distribution of higher channel gains with increasing turbulence, as shown in Fig. 6. At low SNR, the transmitter, assuming full CSI, adapts the beam power optimally, allocating more power to stronger channel gains while avoiding power wastage on weaker states. Consequently, power adaptation yields a net ASE gain at low SNRs, as confirmed by the numerical results in Fig. 5. For instance, at

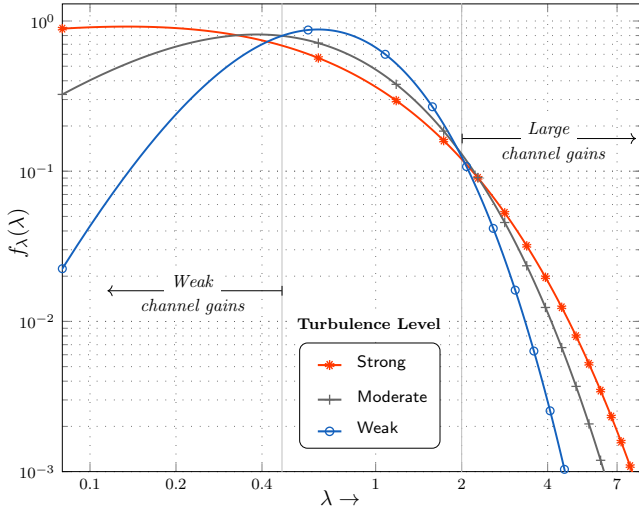


Fig. 6. The PDF of the GG fading gain for the settings described in Table I. Notice the larger probabilities for the higher gains with increasing turbulence.

a target SNR of -10 dB/Hz, the ASE improves from 0.1816 bits/s/Hz under weak turbulence to 0.2434 bits/s/Hz under strong turbulence (34% increase). In a wavelength-division multiplexed (WDM) system with 50 GHz optical bandwidth per channel, this corresponds to an increase from about 9.08 Gb/s to 12.172 Gb/s per channel for the same transmit power budget. Such per-channel low-SNR conditions are not typical in current deployments but may plausibly arise in future ultra-wideband WDM coherent FSO systems where a fixed eye-safety-limited transmit power must be shared among many carriers, with atmospheric variability (e.g., haze or fog) further accentuating this effect. At a lower target SNR of -15 dB/Hz, the ASE increases from about 3.52 Gbps/channel to 5.42 Gbps/channel (53% gain). Moreover, the channel's ASE per unit SNR—known as the wideband slope [51]—improves as the SNR decreases: under strong turbulence it rises from 2.43 units at -10 dB to 3.43 units at -15 dB (41% increase), while under weak turbulence it increases from 1.82 to 2.27 units (25% gain).¹

In contrast, the effect of turbulence on the spectral efficiency of the optical channel with pointing error at low SNRs is more involved. As depicted in Figures 8-7, the spectral efficiency initially shows a slight improvement in the weak-to-moderate turbulence regime, but then begins to degrade as turbulence strength increases from moderate to strong levels. This unusual behavior can be explained using the asymptotic low-SNR spectral efficiency result in (42) from Theorem 2. The combined effect of atmospheric turbulence and pointing error on the optical channel's spectral efficiency at low SNR is encapsulated in the term $A_0/4ab$, which can be rewritten as

$$\text{Scaling factor} \triangleq A_0 \times \frac{1}{4ab}. \quad (56)$$

Fig. 9 illustrates the variation of the scaling factor in (56) (red curve) with turbulence, alongside the factor $1/4ab$ (blue curve), which applies to pure optical turbulence (see (48)). A

¹Here, 'unit' denotes bits/s/Hz per unit SNR, with SNR expressed in linear ratio.

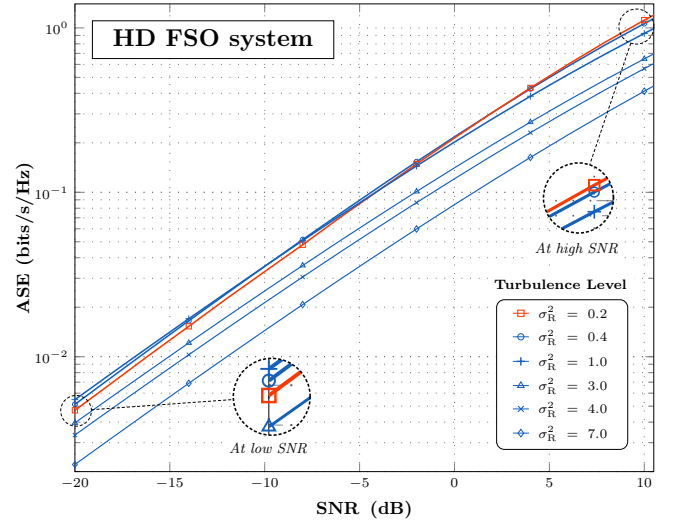


Fig. 7. Spectral efficiency results in the low SNR regime for gamma-gamma turbulence channel with 'mild' pointing jitter under HD detection scheme.

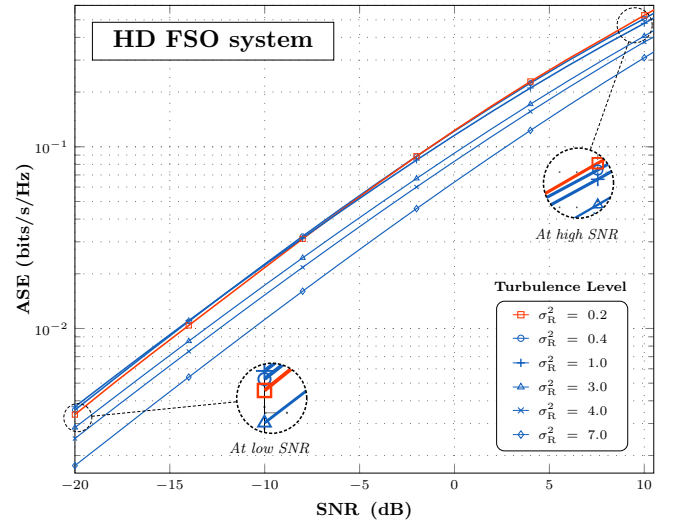


Fig. 8. Spectral efficiency results in the low SNR regime for gamma-gamma turbulence channel with 'strong' pointing jitter under HD detection scheme.

comparison of the two curves reveals that the parameter A_0 , representing the fraction of collected power, decreases with turbulence—initially slowly in the weak fluctuation regime and then more rapidly under strong turbulence, while the factor $1/4ab$ increases. For further insight into how A_0 varies with turbulence, refer to the A_0 values in Table I, which provide typical values for weak, moderate, and strong turbulence conditions. In general, except under weak fluctuations, the spectral efficiency of the channel at low SNR with both fading and pointing error tends to degrade with increasing turbulence over a broad range of moderate-to-strong conditions.

Interestingly, the asymptotic result (42) indicates that the influence of pointing jitter strength ξ^2 on the channel's ASE vanishes in the low-SNR regime: the transmitter operates only during channel peaks, and it can be verified that the distribution of these peaks is largely insensitive to ξ^2 . The low-SNR ASE characterization for mobile RF channels in

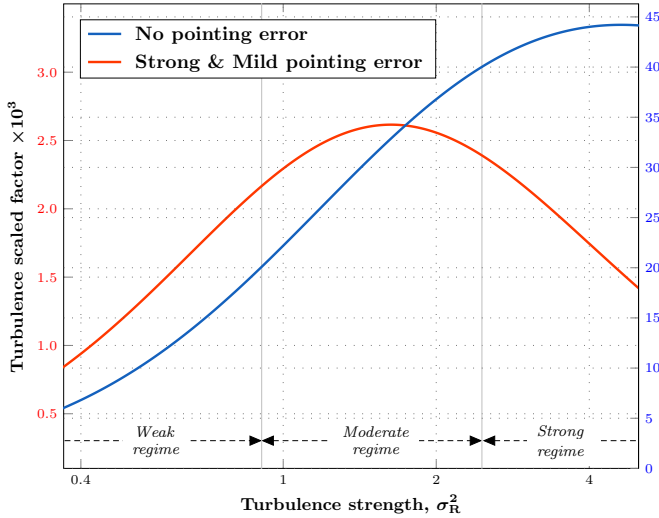


Fig. 9. Variation of the turbulence scaled factor for the GG turbulence channel under HD detection scheme.

[52] reveals two key insights: power adaptation reduces to an asymptotically optimal on–off strategy, and transmitter feedback collapses to a single bit information. These simplifications are expected to carry over to terrestrial optical channels at low SNRs, offering practical benefits for FSO system design.

V. CONCLUSION

In this work, we have analyzed the average spectral efficiency of terrestrial FSO communication systems over gamma-gamma turbulence channels with beam power adaptation incorporated at the optical transmitter side. The analysis also highlighted the detrimental impact on the performance due to pointing errors impairments present in typical FSO links.

The proposed exact solutions capture the impact of fading and pointing error parameters, with particular emphasis on the high and low SNR regimes, and highlight an interplay between A_0 and ξ^2 as turbulence and pointing error conditions vary. Under mild or negligible pointing error condition—typical of practical systems with well-designed ATP—the expected degradation of spectral efficiency with increasing turbulence is observed. In contrast, for channels with strong pointing error condition—typical of systems with poorly designed or absent ATP, which may occur in low-cost deployments—a notable improvement in spectral efficiency is observed at high SNRs as turbulence increases from weak conditions, since the reduction in pointing jitter outweighs the loss in received power. Overall, these results provide insights across the full spectrum of ATP capabilities, from practical well-designed systems to theoretical or low-cost configurations with no or poorly performing ATP.

At low SNRs, we have shown that the average spectral efficiency can improve with turbulence due to two main factors: i) the distribution of higher fading gains improves with turbulence, and ii) the transmitter efficiently exploits these higher gains through beam power control. However, in the presence of pointing error, the distribution of higher gains deteriorates significantly with turbulence, resulting in

a loss of spectral efficiency at low SNRs. From a system design perspective, operation at low SNRs is particularly relevant for terrestrial coherent FSO links for two reasons: first, the stringent per-hertz optical power limitations plausible in future ultra-wideband, long-haul deployments, and second, the superior energy efficiency of wideband communication systems when operated in the power-limited regime. In this light, the spectral efficiency characterization developed in this work provides timely and practically significant insights into the design of next-generation coherent FSO systems.

As future work, the proposed spectral-efficiency framework can be extended to multi-aperture (MIMO) systems, which we identify as a promising direction for advancing research on next-generation terrestrial coherent FSO systems. Similarly, leveraging the derived ASE limits as a reference for analyzing and optimizing practical coherent FSO implementations represents another valuable avenue for further investigation.

REFERENCES

- [1] S. Arnon, J. Barry, G. Karagiannidis, R. Schober, and M. Uysal, *Advanced Optical Wireless Communication Systems*. Cambridge, U.K.: Cambridge Univ. Press, 2012.
- [2] Q. Liu, C. Qiao, G. Mitchell, and S. Stanton, “Optical wireless communication networks for first- and last-mile broadband access,” *IEEE/OSA J. Opt. Netw.*, vol. 4, no. 12, p. 807–828, 2005.
- [3] D. Cornwell, “Laser communication from the Moon at 622Mb/s,” Available: <http://spie.org/x107507.xml>, 2014.
- [4] F. Heine, H. Kämpfner, R. Czichy, R. Meyer, and M. Lutzer, “Optical inter-satellite communication operational,” in *Proc. IEEE Military Communications Conference (MILCOM)*, 2010, pp. 1583–1587.
- [5] H. Haan and M. Tausendfreund, “Free-space optical data transmission for military and civil applications: A company report on technical solutions and market investigation,” in *2013 15th International Conference on Transparent Optical Networks (ICTON)*. IEEE, 2013, pp. 1–4.
- [6] F. P. Guiomar, M. A. Fernandes, J. L. Nascimento, and P. P. Monteiro, “400g+ wireless transmission via free-space optics,” in *2021 European Conference on Optical Communication (ECOC)*, 2021, pp. 1–4.
- [7] M. A. Fernandes *et al.*, “4 Tbps+ fso field trial over 1.8 km with turbulence mitigation and fec optimization,” *Journal of Lightwave Technology*, vol. 42, no. 11, pp. 4060–4067, 2024.
- [8] F. P. Guiomar, M. A. Fernandes, J. L. Nascimento, V. Rodrigues, and P. P. Monteiro, “Coherent free-space optical communications: Opportunities and challenges,” *Journal of Lightwave Technology*, vol. 40, no. 10, pp. 3173–3186, 2022.
- [9] D. J. Heatley, D. R. Wisely, I. Neild, and P. Cochrane, “Optical wireless: The story so far,” *IEEE Communications Magazine*, vol. 36, no. 12, pp. 72–74, 1998.
- [10] J. R. Barry and E. A. Lee, “Performance of coherent optical receivers,” *Proceedings of the IEEE*, vol. 78, no. 8, pp. 1369–1394, 1990.
- [11] L. C. Andrews and R. L. Phillips, *Laser Beam Propagation Through Random Media: Second Edition*. SPIE Press, Bellingham, Washington, 2005.
- [12] S. Bloom, E. Korevaar, J. Schuster, and H. Willebrand, “Understanding the performance of free-space optics,” *Journal of Optical Networking*, vol. 2, no. 6, pp. 178–200, 2003.
- [13] S. Karp, R. M. Gagliardi, S. E. Moran, and L. B. Stotts, *Optical Channels: Fibers, Clouds, Water, and the Atmosphere*. Springer Science & Business Media, 2013.
- [14] M. Al-Habash, L. C. Andrews, and R. L. Phillips, “Mathematical model for the irradiance probability density function of a laser beam propagating through turbulent media,” *Optical Engineering*, vol. 40, no. 8, pp. 1554–1562, 2001.
- [15] A. A. Farid and S. Hranilovic, “Outage capacity optimization for free-space optical links with pointing errors,” *Journal of Lightwave Technology*, vol. 25, no. 7, pp. 1702–1710, 2007.
- [16] F. Yang, J. Cheng, and T. A. Tsiftsis, “Free-space optical communication with nonzero boresight pointing errors,” *IEEE Transactions on Communications*, vol. 62, no. 2, pp. 713–725, 2014.

- [17] A. Jurado-Navas, J. M. Garrido-Balsells, J. F. Paris, A. Puerta-Notario, and J. Awrejcewicz, "A unifying statistical model for atmospheric optical scintillation," in *Numerical Simulations of Physical and Engineering Processes*. Intech Rijeka, Croatia, 2011, vol. 181, no. 8, pp. 181–205.
- [18] M. A. Kashani, M. Uysal, and M. Kavehrad, "A novel statistical channel model for turbulence-induced fading in free-space optical systems," *Journal of Lightwave Technology*, vol. 33, no. 11, pp. 2303–2312, 2015.
- [19] K. P. Peppas, G. C. Alexandropoulos, E. D. Xenos, and A. Maras, "The fisher–snedecor \mathcal{F} -distribution model for turbulence-induced fading in free-space optical systems," *Journal of Lightwave Technology*, vol. 38, no. 6, pp. 1286–1295, 2020.
- [20] International Electrotechnical Commission, "IEC 60825-1:2014 - Safety of Laser Products – Part 1: Equipment Classification and Requirements," International standard, 3rd Edition, 2014. Available: <https://webstore.iec.ch/publication/6049>.
- [21] A. Dochhan, J. Poliak, J. Surof, M. Richerzhagen, H. F. Kelemu, and R. M. Calvo, "13.16 Tbit/s free-space optical transmission over 10.45 km for geostationary satellite feeder-links," in *Photonic Networks: 20th ITG-Symposium*, 2019, pp. 1–3.
- [22] S. T. Hong and A. Ishimaru, "Two-frequency mutual coherence function, coherence bandwidth, and coherence time of millimeter and optical waves in rain, fog, and turbulence," *Radio Science*, vol. 11, no. 6, pp. 551–559, 1976.
- [23] H. Lu, W. Zhao, and X. Xie, "Analysis of temporal broadening of optical pulses by atmospheric dispersion in laser communication system," *Optics Communications*, vol. 285, no. 13, pp. 3169–3173, 2012.
- [24] A. Mostafa and S. Hranilovic, "Channel measurement and markov modeling of an urban free-space optical link," *Journal of Optical Communications and Networking*, vol. 4, no. 10, pp. 836–846, 2012.
- [25] W. Gappmair, "Further results on the capacity of free-space optical channels in turbulent atmosphere," *IET Communications*, vol. 5, no. 9, pp. 1262–1267, 2011.
- [26] M. Z. Hassan, M. J. Hossain, and J. Cheng, "Ergodic capacity comparison of optical wireless communications using adaptive transmissions," *Opt. Express*, vol. 21, no. 17, pp. 20 346–20 362, Aug 2013.
- [27] F. Benkhelifa, Z. Rezki, and M.-S. Alouini, "Low snr capacity of FSO links over gamma-gamma atmospheric turbulence channels," *IEEE Communications Letters*, vol. 17, no. 6, pp. 1264–1267, 2013.
- [28] I. S. Ansari, F. Yilmaz, and M.-S. Alouini, "Performance analysis of FSO links over unified gamma-gamma turbulence channels," in *IEEE 81st Vehicular Technology Conference (VTC Spring)*, Glasgow, UK, 2015, pp. 1–5.
- [29] I. E. Lee, Z. Ghassemloooy, W. P. Ng, M.-A. Khalighi, and S.-K. Liaw, "Effects of aperture averaging and beam width on a partially coherent Gaussian beam over free-space optical links with turbulence and pointing errors," *Applied Optics*, vol. 55, no. 1, pp. 1–9, 2016.
- [30] H. E. Nistazakis, E. A. Karagianni, A. D. Tsigopoulos, M. E. Fafalios, and G. S. Tombras, "Average capacity of optical wireless communication systems over atmospheric turbulence channels," *Journal of Lightwave Technology*, vol. 27, no. 8, pp. 974–979, 2009.
- [31] H. AlQuwaiee, I. S. Ansari, and M.-S. Alouini, "On the performance of free-space optical communication systems over double generalized gamma channel," *IEEE Journal on Selected Areas in Communications*, vol. 33, no. 9, pp. 1829–1840, 2015.
- [32] I. S. Ansari, M.-S. Alouini, and J. Cheng, "Ergodic capacity analysis of free-space optical links with nonzero boresight pointing errors," *IEEE Transactions on Wireless Communications*, vol. 14, no. 8, pp. 4248–4264, 2015.
- [33] O. S. Badarneh, R. Derbas, F. S. Almeahmadi, F. El Bouanani, and S. Muhaidat, "Performance analysis of fso communications over \mathcal{F} turbulence channels with pointing errors," *IEEE Communications Letters*, vol. 25, no. 3, pp. 926–930, 2021.
- [34] Y. M. Shishter, F. H. Ali, and R. C. Young, "Performance analysis of fso communications over a generalized turbulence fading channel with pointing error," *Transactions on Emerging Telecommunications Technologies*, vol. 35, no. 2, p. e4935, 2024.
- [35] H. Weichel, *Laser Beam Propagation in the Atmosphere*. SPIE Optical Engineering Press, Bellingham, 1990.
- [36] I. S. Gradshteyn and I. M. Ryzhik, *Table of Integrals, Series, and Products*, 7th ed. San Diego, CA: Academic Press, Inc., 2007.
- [37] B. E. Saleh and M. C. Teich, *Fundamentals of Photonics*. John Wiley & Sons, Ltd, 2019.
- [38] J. C. Ricklin and F. M. Davidson, "Atmospheric turbulence effects on a partially coherent Gaussian beam: implications for free-space laser communication," *Journal of the Optical Society of America A, Optics, Image Science, and Vision*, vol. 19, no. 9, pp. 1794–1802, Sept. 2002.
- [39] A. È. Siegman, *Lasers*. Mill Valley, CA, USA: University Science Books, 1986.
- [40] M. Miao, X.-y. Chen, R. Yin, and J. Yuan, "New results for the pointing errors model in two asymptotic cases," *IEEE Photonics Journal*, vol. 15, no. 3, pp. 1–7, 2023.
- [41] B. Oliver, "Thermal and quantum noise," *Proceedings of the IEEE*, vol. 53, no. 5, pp. 436–454, 1965.
- [42] G. P. Agrawal, *Fiber-Optic Communication Systems*, 3rd ed. New York: Wiley, 2002.
- [43] J. Kahn and J. Barry, "Wireless infrared communications," *Proceedings of the IEEE*, vol. 85, no. 2, pp. 265–298, 1997.
- [44] S. M. Moser, "Capacity results of an optical intensity channel with input-dependent Gaussian noise," *IEEE Transactions on Information Theory*, vol. 58, no. 1, pp. 207–223, 2012.
- [45] K. Kikuchi, "Fundamentals of coherent optical fiber communications," *Journal of Lightwave Technology*, vol. 34, no. 1, pp. 157–179, 2015.
- [46] A. Chaaban, Z. Rezki, and M.-S. Alouini, "On the capacity of intensity-modulation direct-detection Gaussian optical wireless communication channels: A tutorial," *IEEE Communications Surveys & Tutorials*, vol. 24, no. 1, pp. 455–491, 2021.
- [47] E. A. Lee and D. G. Messerschmitt, *Digital Communication*. Springer Science & Business Media, 2012.
- [48] A. Lapidoth, S. M. Moser, and M. A. Wigger, "On the capacity of free-space optical intensity channels," *IEEE Transactions on Information Theory*, vol. 55, no. 10, pp. 4449–4461, 2009.
- [49] Wolfram Research, Inc., "The Wolfram Functions website." Available: <https://functions.wolfram.com/07.34.21.0002.01>.
- [50] R. R. Beland, *Propagation through Atmospheric Optical Turbulence. The Infrared and Electro-Optical Systems Handbook*, F. G. Smith, ed. (SPIE Optical Engineering Press, Bellingham, Washington), Vol. 2, Chap. 2, 1993.
- [51] S. Verdu, "Spectral efficiency in the wideband regime," *IEEE Transactions on Information Theory*, vol. 48, no. 6, pp. 1319–1343, 2002.
- [52] A. Tall, Z. Rezki, and M.-S. Alouini, "Mimo channel capacity with full csi at low snr," *IEEE Wireless Communication Letters*, vol. 1, no. 5, pp. 488–491, 2012.